International Association
Bridge Earthquake Engineering

The Third International Bridge Seismic Workshop, 3rd IBSW

Seattle, Washington, USA - October 1st to 4th, 2019

EFFECT OF DESIGN DETAILS ON SEISMIC RESPONSE OF RC BRIDGE COLUMNS UNDER LONG DURATION GROUND MOTIONS

S.M. Alian [(1)], M.A. Moustafa [(2)*], D.H. Sanders [(3)]

[(1)] *Graduate Student, University of Nevada, Reno, alian@nevada.unr.edu*
[(2)] *Assistant Professor, University of Nevada, Reno, mmoustafa@unr.edu (*Corresponding and Presenting Author)*
[(3)] *Professor and Chair, Iowa State University, sandersd@iastate.edu*

Abstract

Devastating long-duration earthquakes such as 2011 Tohoku Earthquake in Japan, and 2010 Chile Earthquake have proved the importance of considering ground motion duration for seismic demand assessment. Thus, it is important to understand the design implications of long duration earthquakes. This paper focuses on using experimental methods to study the effect of different reinforcement and design details on the seismic response of reinforced concrete (RC) bridge columns under long duration ground motions. Three large-scale RC bridge columns are tested under the same long duration earthquake record at one of the shake tables at the University of Nevada, Reno. The three columns have different design details but all tested under uniaxial excitation using one of the 2011 Tohoku earthquake records. The specific objective of the shake table tests is to study the effect of varying confinement, i.e. transverse reinforcement, and the use of longitudinal reinforcement debonding in the plastic hinge zone on the seismic capacity of the columns. All three columns have same longitudinal reinforcement ratio. However, two columns have different confinement and transverse reinforcement ratios, while the third column considers debonding of longitudinal reinforcement in the plastic hinge zone. The results of the shake table tests and a comparison of the global and local seismic response of the three columns are presented in this paper. The global response includes the force and displacement capacities and mode of failure. On the other hand, the presented local response includes the strain in both transverse and longitudinal rebars and the columns' curvature within the plastic hinge zone. The test results can help assess the effectiveness of the varied design details, i.e. confinement and debonding, and provide a foundation for future design guidelines to account for longer duration earthquakes.

Keywords: Long duration earthquakes; reinforced concrete; bridge columns; confinement; debonding

1. Introduction

Previous earthquakes such as 2011 Tohoku-Japan Earthquake and 2010 Chile Earthquake have shown the importance of the ground motion duration on seismic performance of structures. However, current seismic design codes do not explicitly take earthquake duration into consideration.

Kunnath et al. investigated cumulative damage in twelve 1/4-scale RC circular bridge columns using a series of monotonic and cyclic excitations through an experimental study [1]. Failure mode in the columns subjected to large displacement amplitudes in excess of 5% drift, was longitudinal bar rupture due to low cycle fatigue, while under larger number of smaller amplitude cycles, confinement failure due to spiral rupture was observed. Proper confinement

Ranf et al. tested six identical RC circular bridge columns to evaluate the effect of number of cycles on damage progression [2]. The columns were lightly confined and tested under cyclic loadings. The results showed 30% reduction in the maximum displacement at the final damage states by increasing the number of cycles from 1 to 15 at each displacement level.

Ou et al. studied seismic behavior of flexural-dominated RC bridge columns under long-duration motions. Two identical columns were tested using two cyclic loading protocol [3]. The former was representing the number of cycles expected in a long duration earthquake, while the later was a baseline loading protocol with one cycle for each drift loading. The main observation was 24% reduction in ductility capacity for the column subjected to the long duration loading protocol.

Mohammed et al. investigated the effect of earthquake duration on collapse capacity of RC bridge columns [4]. Shake table tests were conducted for five 1/3-scale identical columns under a loading protocol utilizing a sets of five spectrally similar or close ground motions including one short duration and four long duration motions. The experimental study showed a significant effect of duration on the collapse capacity of the columns. Longitudinal bars in the columns subjected to the longer motions were fractured at lower displacements (32% lower) compared to the one under the short duration motion.

2. Specimens Description

Three 1/3-scale cast-in-place (CIP) reinforced concrete (RC) bridge column models were constructed and tested on a shake table at the University of Nevada, Reno. The test specimens were adopted from a previous study by Phan et al. [5], in which columns were designed based on AASHTO (2002) [6]. The design still meets the requirements of AASHTO (2014) [7].

Fig. 1 shows the dimension details for all specimens. The columns were circular with 16 in. diameter and clear height of 72 in. Axial load was 80 kips which corresponded to 8% of column axial capacity. Columns had similar geometry and longitudinal bar arrangements. Table 1 lists reinforcement details of the specimens. The longitudinal reinforcement was 22 #4. The reference column had transverse steel ratio of 1.04% (#3@3”). This column will hereafter be referred to as LD-S3-G60. In the second column (LD-S1.5-G60), the transverse steel ratio was doubled (2.08%, #3@1.5”) to investigate the effect of transverse bar spacing on column seismic performance. In the third column (LD-S3-G60D), transverse steel was the same as the reference column, but longitudinal bars were debonded at column-footing interface with an intent to spread the bar yielding and to potentially enhance the displacement capacity.

All columns were designed to behave as cantilever columns to be representative of single-column bridge piers. The columns also had equal moment capacity. The footings were designed to be stiff enough to prevent any footing damage and to provide adequate fixity for the cantilever column.

Table 1 – Specimens reinforcement details

Specimens	**LD-S3-G60**	**LD-S1.5-G60**	**LD-S3-G60D**
Long. Reinforcement	22 #4 (2.2%) Gr. 60	22 #4 (2.2%) Gr. 60	22 #4 (2.2%) Gr. 60
Trans. Reinforcement	#3 @ 3 in. (1.04%)	#3 @ 1.5 in. (2.08%)	#3 @ 3 in. (1.04%)
Tie Spacing	6 d_b	3 d_b	6 d_b

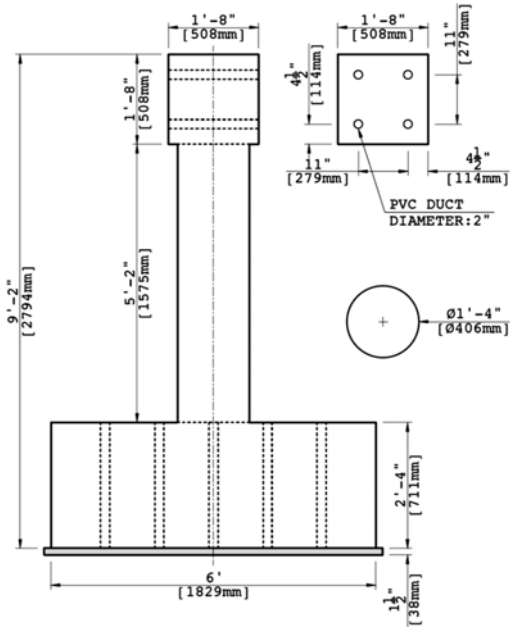

Fig. 1 – Dimension details of the specimens

Longitudinal and transverse reinforcement in all specimens were ASTM A706 Grade 60. Table 2 lists the measured properties of steel reinforcement. Table 3 lists 7-day, 28-day, and test-day properties of concrete. In order to make direct comparisons. All three specimens were constructed simultaneously.

Table 2 – Longitudinal reinforcing steel properties

F_y (ksi)	ε_y	E (ksi)	ε_{sh}	E_{sh}	F_{max} (ksi)	ε_{Fmax}	F_u (ksi)	ε_u
72.3	0.0025	29000	0.0045	1100	113.3	0.092	100	0.144

Table 3 – Concrete compressive strength

7 days (ksi)	28 days (ksi)	Test day (ksi)		
		107 days LD-S3-G60	120 days LD-S1.5-G60	126 days LD-S3-G60D
3.31	5.24	7.22	7.31	7.77
3.18	4.28			5.92

3. Experimental Program

3.1 Test Setup

Figure 2 shows a schematic view of the test setup. Input ground motion was applied uniaxially in the north-south direction of the shake table. Columns were fixed to the footing but free at the top. Footing was fixed to the shake table through 14 high strength, 1 in. diameter threaded rods. Each specimen was attached laterally to a mass rig system that represented the inertial mass. The mass rig was connected to the column head using a rigid link to apply the lateral force to the specimen. Four threaded high strength rods were used to connect the head of the column with the rigid link. A constant axial force of 80 kips was applied for each specimen during the tests through a steel spreader beam, two hydraulic jacks, accumulator, and two threaded high strength steel rods (Fig. 1). Steel rods were connected to the jacks and extended through the PVC pipes in the footing and anchored beneath the footing. The hydraulic jacks applied the axial load and the beam transferred it to the specimen. The accumulator was used to keep the axial load constant. Furthermore, the inertial mass

was provided by three concrete blocks each of approximate weight of 20 kips in addition to the mass rig with an effective weight of 20 kips.

3.2 Instrumentation

Various aspects of the specimen behavior were monitored using 110 channels of data. These channels included strain gauges that were installed on seven levels of the extreme northern and southern bars to track strain in the longitudinal bars and spirals, the extent of yielding in the longitudinal bars, and the length of the potential plastic hinge at the base of the column. Novotechnik displacement transducers were used at four levels of the columns to measure curvature and bond slip in the plastic hinge. String potentiometers and load cells were installed on the test model to measure the absolute displacements and base shear. Three tri-axial accelerometers were placed on the footing, at the center of the loading head and on the mass rig to measure accelerations.

3.3 Loading Protocol

The loading protocol for all the columns started with 100% of the Tohoku earthquake recorded at MYG006 E-W station with significant duration (5-95%) of 115 seconds, followed by an aftershock from the Mw 7.1 earthquake that occurred in Japan one month after the Tohoku earthquake. Peak ground accelerations for the main motion and the aftershock were 0.42g and 0.41g, respectively. 125% and 150% of the main motion were then applied to the test model. For the second column an extra run as 160% of the main motion was also applied. The time axis of the records was compressed by a factor of 0.577 corresponding to the square root of the dimensional scale length factor to account for the similitude requirements. White noise tests with frequency content from 0.5 Hz to 30 Hz were conducted before each run and after the last run to determine changes in the fundamental period of the columns due to the progression of damage.

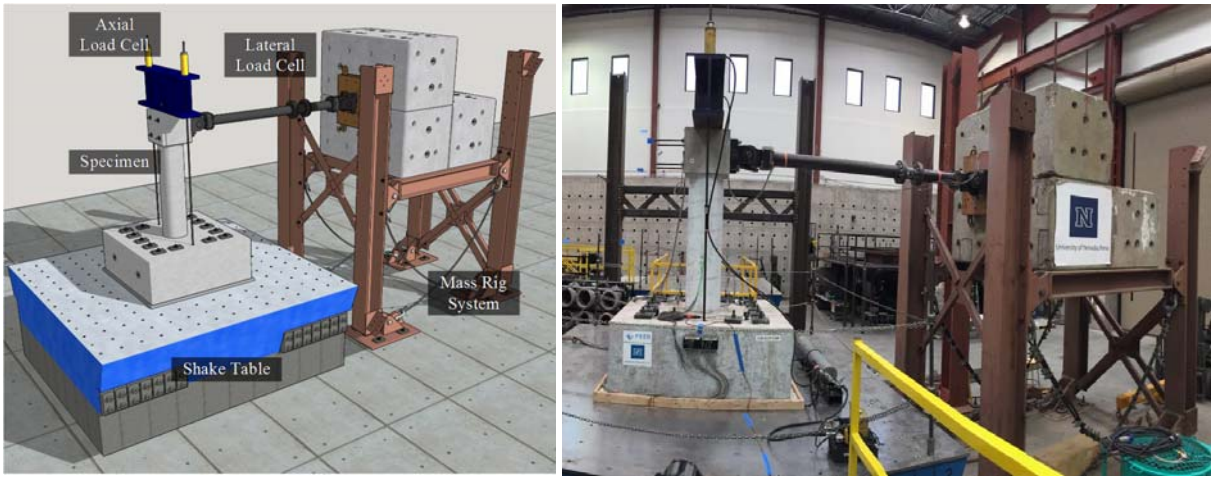

Fig. 2 – Shake table test setup at UNR

4. Experimental Results

4.1 Damage Observations

Four cameras were used to monitor the progression of damage in the columns as well as visual inspections after each run. The damage was concentrated at the columns plastic hinges. Similar damage progression was observed for all columns. The observed behavior of the columns is discussed in the following paragraphs.

LD-S3-G60 – Damage in the column started with flexural cracks and yielding in the longitudinal reinforcement, followed by major spalling of the cover concrete in the first run. No further damage was observed during the second run. In the third run, the core concrete spalling started, and the longitudinal bars buckled. Finally, the damage expanded in the core concrete, and eight longitudinal bars fractured in the 4th run.

LD-S1.5-G60 – Detected damages in two first runs were same as previous column. Cover spalling progressed along the plastic hinge, and spiral was exposed during the third run. After the fourth run, the damage state remained as previous run. In the fifth run, the longitudinal bars were exposed, and one bar fractured.
LD-S3-G60D – Same as previous columns, major spalling observed in the first and second runs. In the third run, spalling progressed thorough the core concrete, longitudinal bars buckled, and two bars ruptured. Since the bar fractures happened after the strong part of the motion, the fourth run was also applied. Eight more bars fractured in this run.
Fig. 3 shows the ultimate damage state of the columns after the last run. The footing and loading head were also examined for any damage during the test. No damage was detected except minor spalling on the footing of LD-S1.5-G60.

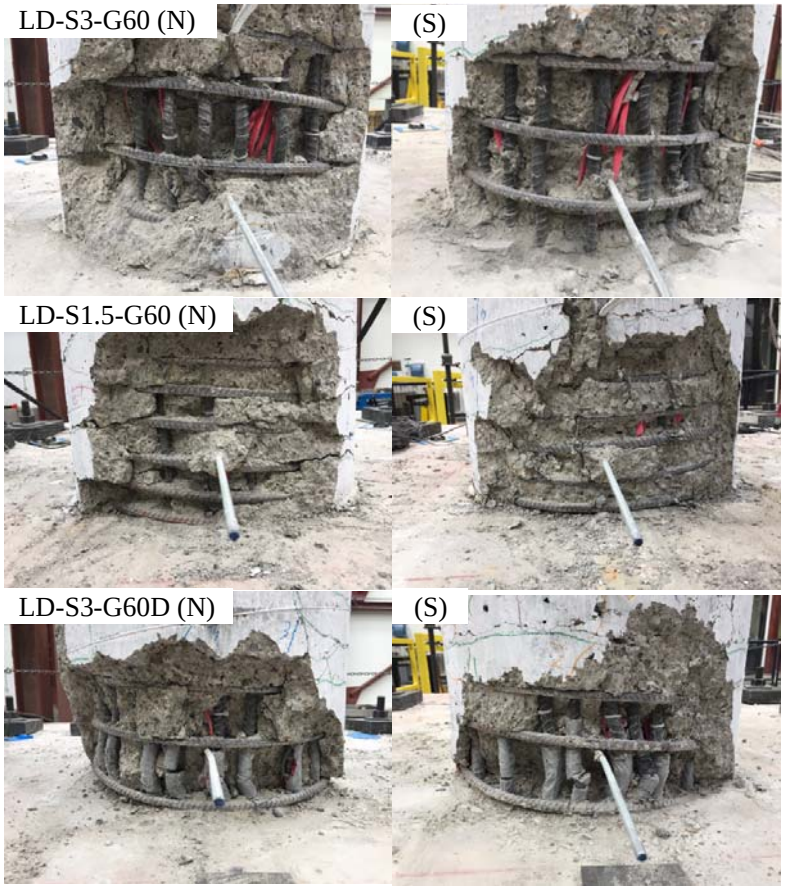

Fig. 3 – Ultimate damage state of the columns

4.2 Achieved Motions

The achieved motions differed from the target ground motions as a result of the interaction between the shake table and the specimen [8]. PGA values for the achieved motions for each test model and for each run are listed in Table 4. Also shown in the table are the PGA values normalized to the PGA of the first run. The parameters to compare the target and achieved motions were the ratio of the achieved to target PGA (Ach./Targ. PGA), and root mean square error ($RMSE_{Sa}$) of the spectral acceleration responses (Table 4). As shown in the table, for the first test model the errors were higher; however, in the subsequent experiments the achieved motions were closer to the target motions.

Table 4 – Achieved and target motions

	LD-S3-G60				LD-S1.5-G60					LD-S3-G60D			
	1	**2**	**3**	**4**	**1**	**2**	**3**	**4**	**5**	**1**	**2**	**3**	**4**
Ach. PGA (g)	0.41	0.37	0.56	0.62	0.41	0.39	0.53	0.61	0.66	0.40	0.43	0.52	0.59
Norm. PGA	1.00	0.90	1.36	1.51	1.00	0.95	1.28	1.48	1.60	1.00	1.07	1.30	1.48
Ach./Targ. $_{PGA}$	0.98	0.78	1.06	0.99	0.98	0.82	1.01	0.97	0.98	0.95	0.89	0.99	0.94
$RMSE_{Sa}$ (g)	0.15	0.14	0.12	0.11	0.08	0.11	0.04	0.04	0.03	0.05	0.08	0.03	0.06

4.3 Force-Displacement Relationships

The absolute lateral displacement of the column at the centerline of the loading head was estimated from measured displacements of three corners of the loading head. The relative displacement (hereafter referred to as column displacement) was determined by subtracting the shake table displacement from the absolute displacement. Drift ratios were determined by dividing the relative displacements to the column clear height. The peak displacements of the columns, their respective drift ratios and residual drift ratios in each run are listed in Table 5.

Since the columns behaved like a single degree of freedom structure, the base shear was measured directly from the load cell located on the mass rig link. The peak base shear and bending moment of the columns in each run are listed in Table 5.

Fig. 4 shows the peak drift ratios and base shears in each run. It is evident that the second specimen with higher confinement represents the highest displacement capacity. The second column demonstrated higher displacement capacity compared to the first one as a result of the debonding of the longitudinal bars.

Table 5 – Responses of the columns

	LD-S3-G60				LD-S1.5-G60					LD-S3-G60D			
	1	**2**	**3**	**4**	**1**	**2**	**3**	**4**	**5**	**1**	**2**	**3**	**4**
Peak Disp. (in.)	4.41	2.80	5.95	6.44	4.57	2.71	7.56	8.93	10.0	4.72	2.77	6.83	7.99
Peak Drift (%)	6.13	3.89	8.27	8.94	6.35	3.76	10.5	12.4	13.9	6.56	3.85	9.48	11.1
Res. Drift (%)	0.47	0.57	0.59	1.18	0.57	0.46	1.58	2.99	5.60	0.14	0.22	0.07	0.53
Peak Base Shear (kips)	35.7	25.1	38.8	36.7	35.4	26.1	36.1	35.9	35.6	33.6	26.0	33.4	21.1
Peak Bending Moment (kip.ft)	214	151	233	220	212	157	217	215	214	202	156	200	127

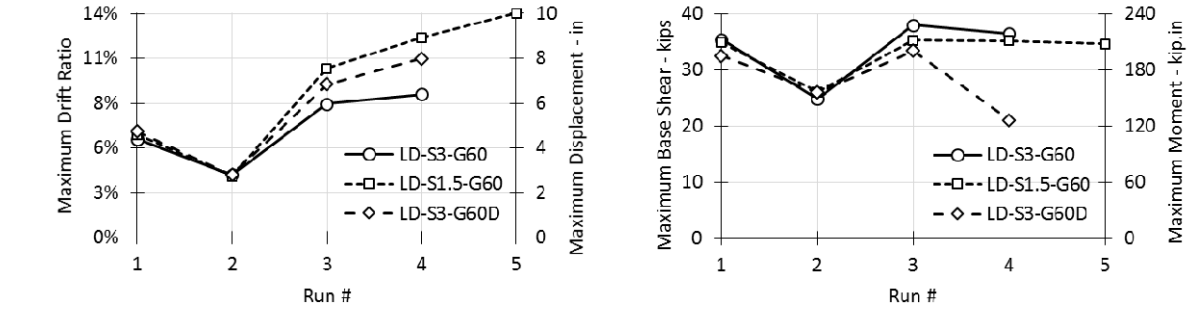

(a) (b)

Fig. 4 – Peak columns (a) drift ratios and (b) forces in each run

The hysteresis relationship between the columns base shear and displacement was studied to assess the overall force-displacement relationship of the columns. The measured envelopes of the cumulative hysteresis curves

were idealized by elasto-plastic curves passing through the first column longitudinal bar yielding and adjusted to preserve energy. Fig. 5 represents the cumulative force-displacement relationship of the columns along with the envelopes and their respective idealized curves. Wide hysteresis loops of all three columns indicate a good energy dissipation.

The idealized curve for the dominant direction was used to calculate the displacement ductility and the initial effective stiffness (Fig. 5d). Displacement ductility was obtained by dividing the ultimate column drift ratio to the effective yield drift ratio. The first yielding of the longitudinal bars occurred at drift ratios of 1.03% (LD-S3-G60), 1.10% (LD-S1.5-G60), and 1.18% (LD-S3-G60D). The ultimate drift ratios were determined based on the onset of the bar fractures. The displacement ductility of the three test models were 5.60%, 8.14%, and 5.35%, respectively. The slope of the elastic branch of the idealized curve was considered as the initial effective stiffness of the columns resulting in 30.3, 27.2, and 24.4 kip/in for the three columns, respectively.

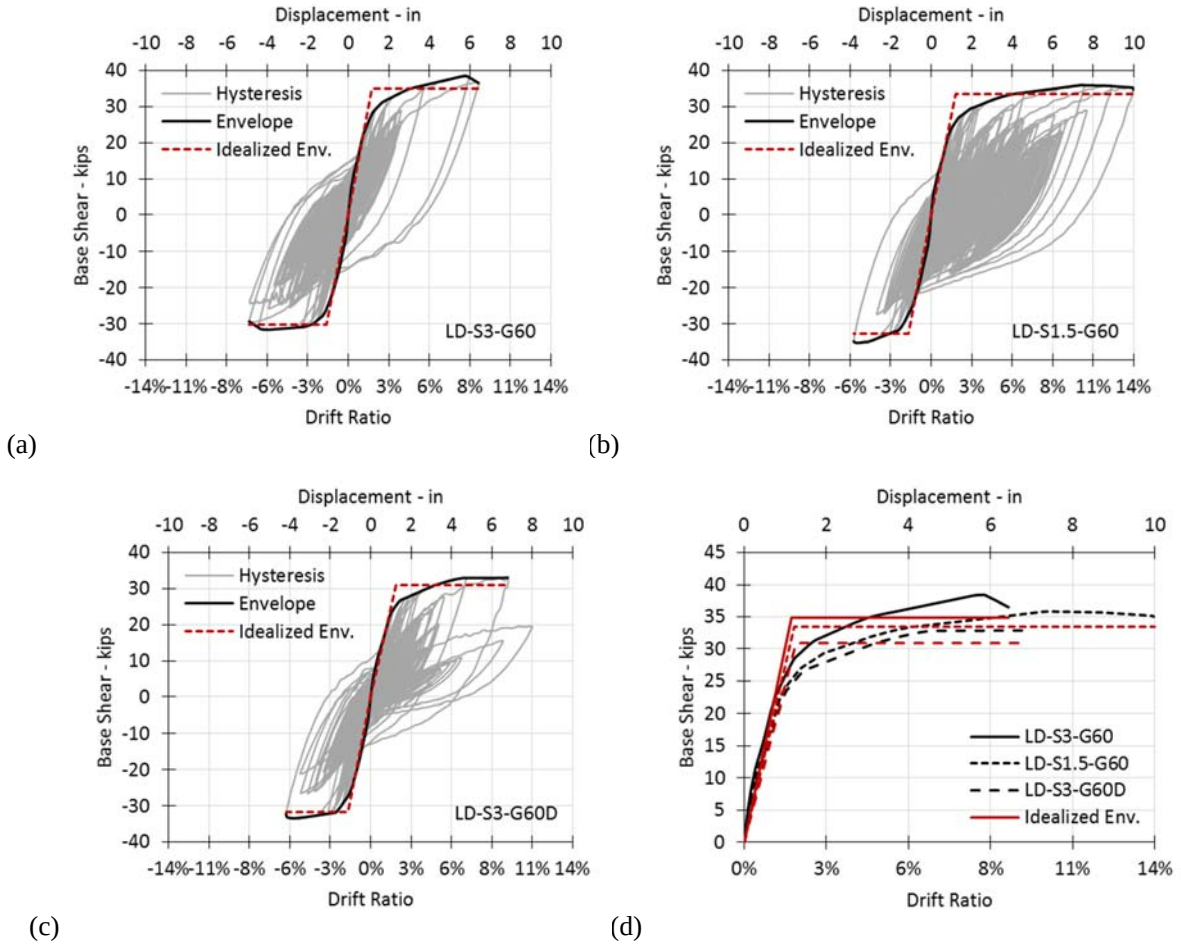

Fig. 5 – Cumulative force-displacement relationships, envelops and idealized envelops

4.4 Periods

The fundamental frequencies of the columns were estimated using Fast Fourier Transform (FFT) of the measured acceleration at the tip of the columns during white noise tests. The resulting periods are shown in Fig. 6a. Fig. 6b shows effective periods for each run based on the slope of the linear fitting of the hysteresis force-displacement relationship (as K_{eff}) and the seismic weight of the test model (80 kip). Furthermore, the initial slope of the idealized force-displacement curves (section 4.3) resulted in initial periods of 0.52, 0.55,

and 0.58 sec for the LD-S3-G60, LD-S1.5-G60 and LD-S3-G60D test models, respectively. Both figures clearly show the elongation of the periods for all the test models as nonlinearity spreads in the column plastic hinge. Higher periods of the LD-S3-G60D is an indicator of the more damages in this column.

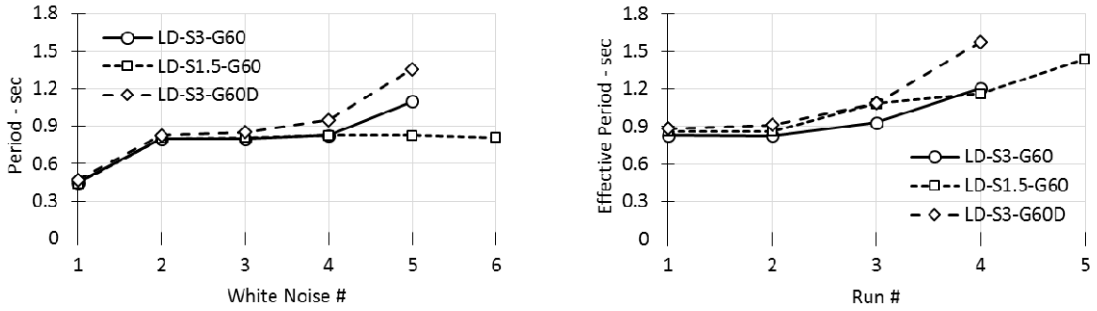

(a) (b)

Fig. 6 – Measured periods from (a) white noise tests and (b) linear fit

4.5 Strains

Strain profiles in Fig. 7 represent the peak measured strains of the extreme northern and southern longitudinal bars at each level of the column plastic hinges as a ratio of the yield strain. The gray points of the strain profiles were not recorded properly due to malfunction of the strain gauges and were estimated based on the data of the other strain gauges. The figures show that the interface strains are the largest as expected. For the second specimen (LD-S1.5-G60), strains are better distributed along the length of the plastic hinge which is attributed to the higher confinement. For the third specimen, strain concentration in the vicinity of the column-footing interface was reduced compared to the first two specimens as a result of the debonding of the longitudinal bars at the interface. Fig. 8 shows the peak strain of the longitudinal bars for each column and for each run. Strain values for the runs in which rupture happened are not shown. Column LD-S1.5-G60 shows higher strain ductility compared to the other two columns, while LD-S3-G60D shows the lowest strain ductility. The maximum measured strain in the spirals for the three test models were 1.8, 0.8, and 1.7 of the yield strain, respectively, so no yielding happened in the spirals.

4.6 Bond-slip Rotations and Curvature Profiles

Bond slip rotations and curvatures were obtained based on the measured data by Novotechnics, the measured gauge length, and the distance of each Novotechnic rod to the face of the columns. Fig. 9 demonstrates the column curvature profile along the length of the plastic hinge. As shown, for all the specimens the curvature was more concentrated at the column-footing interface and to some extent over the plastic hinge length for the first and second columns (LD-S3-G60 and LD-S1.5-G60). The maximum curvature for the three columns were 0.016, 0.018, and 0.028 /in, respectively.

Peak bond slip rotations during each run are presented in Fig. 10. Higher rotational capacity of the last specimen due to the intentional debonding of the longitudinal bars is evident in the diagram.

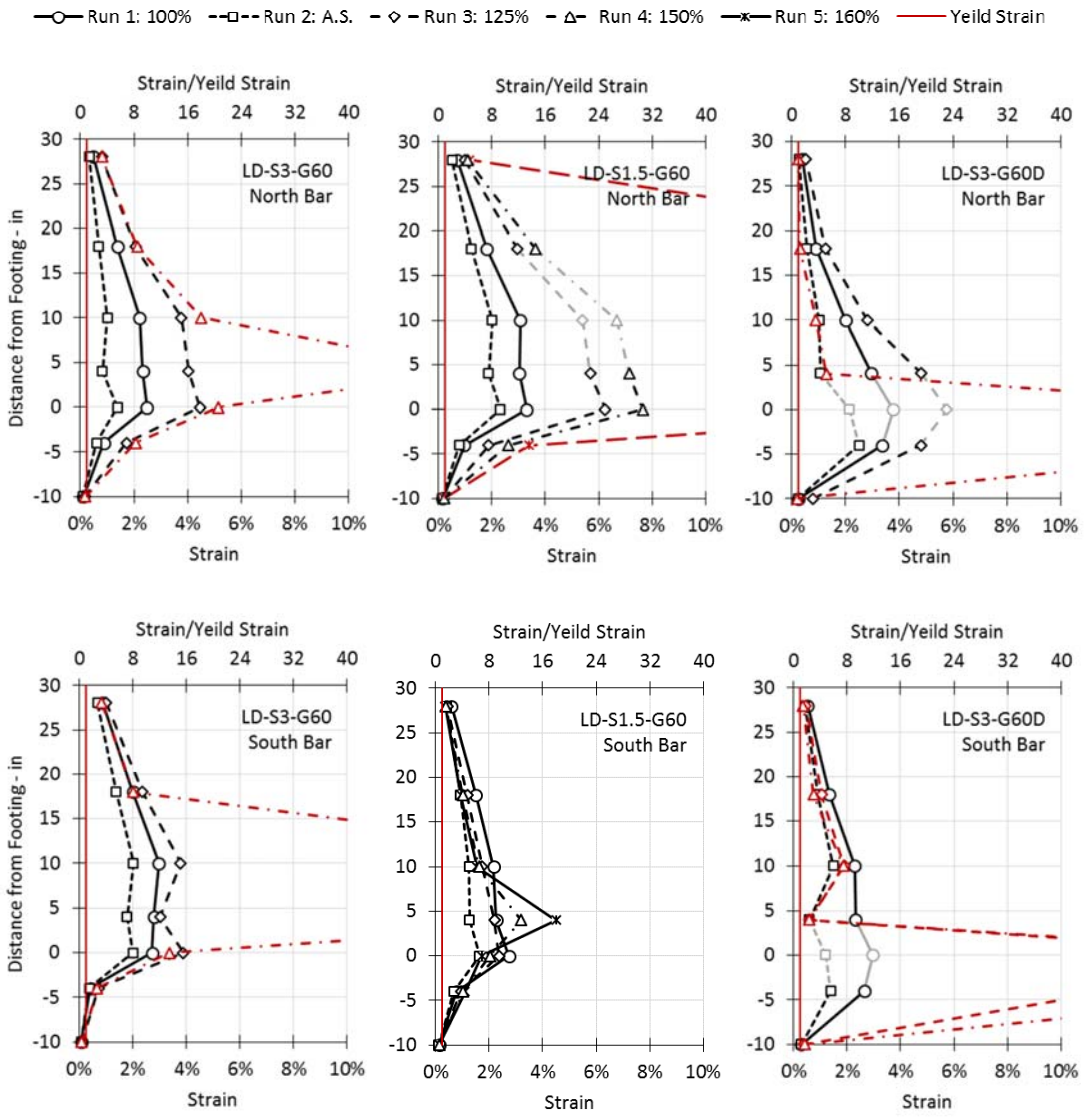

Fig. 7 – Strain profile of the longitudinal bars for each column

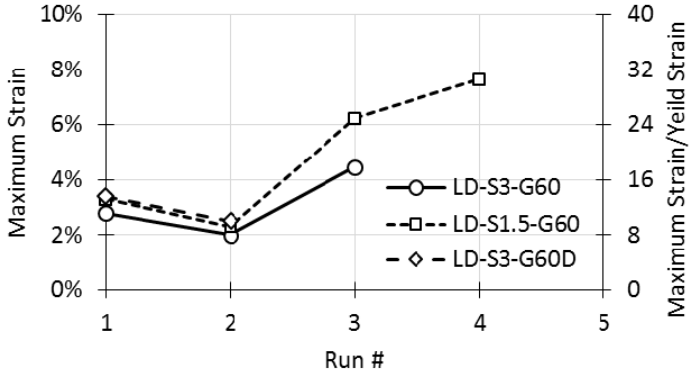

Fig. 8 – Peak strain of the longitudinal bars for each column

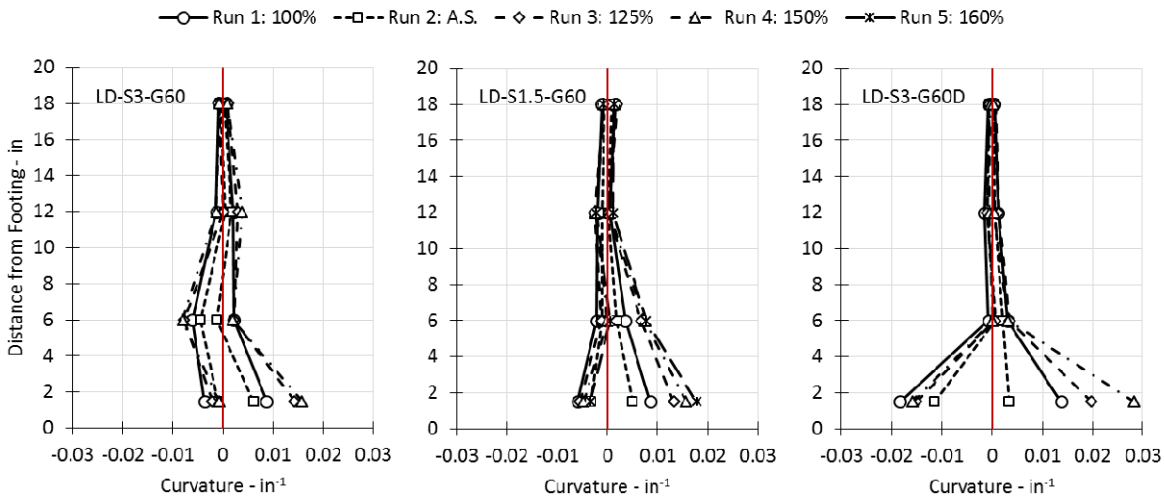

Fig. 9 – Curvature profile along the plastic hinge

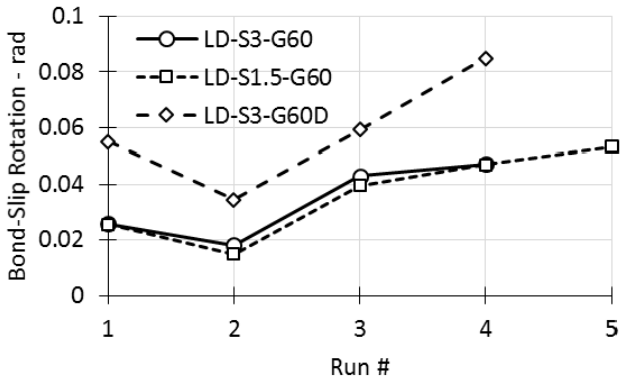

Fig. 10 – Peak bond slip rotations in each run

6. Summary and Conclusions

This study aimed to investigate the effect of various design details on seismic response of RC bridge columns under long duration motions. Three large-scale columns were tested under the same long duration earthquake record on a shake table. The effect of transverse steel spacing and longitudinal bar debonding in the plastic hinge zone were specifically studied.

The seismic performance of the columns was satisfactory. All columns performed in a ductile manner and underwent significant displacements. A good energy dissipation was observed based on the wide hysteresis force-displacement relationship loops. As intended, the columns had flexural-dominated behavior, and the damage was concentrated in the plastic hinges. The failure mode was flexural due to longitudinal bars fracture dictated by low-cycle fatigue.

Using smaller spacing for transverse reinforcement significantly helped improve the column performance with about 50% larger displacement capacity under long duration motions. Debonding the longitudinal bars at the column-footing interface was less effective with about 20% increase in displacement capacity which was due to the spread of yielding in the plastic hinge zone.

The varied design/detailing parameters affect only the seismic performance of the columns in the nonlinear range, i.e. initial stiffness and first yield were same for all cases.

7. Acknowledgements

This project was supported by the Pacific Earthquake Engineering Research (PEER) center. The authors would like to thank the UNR Earthquake Engineering Laboratory staff Dr. Patrick Laplace, Chad Lyttle, Todd Lyttle, and Mark Lattin for their unfailing support and assistance.

8. References

[1] Kunnath, S. K., El-Bahy, A., Taylor, A., & Stone, W. (1997). Cumulative seismic damage of reinforced concrete bridge piers. No. NCEER-97-0006. National Institute of Standards and Technology (US).

[2] Ranf, R. T., Nelson, J. M., Price, Z., Eberhard, M. O., and Stanton, J. F., (2006). Damage accumulation in lightly confined reinforced concrete bridge columns. Technical Report PEER 2005/08, Pacific Earthquake Engineering Research Center, Berkeley, USA.

[3] Ou, Y. C., Song, J., Wang, P. H., Adidharma, L., Chang, K. C., & Lee, G. C. (2013). Ground motion duration effects on hysteretic behavior of reinforced concrete bridge columns. *Journal of Structural Engineering*, 140(3), 04013065.

[4] Mohammed, M., and Sanders, D., (2016). Effect of Earthquake Duration on Reinforced Concrete Bridge Columns. Ph.D. Dissertation, University of Nevada, Reno, Nevada.

[5] Phan, V., Saiidi, M. S., and Anderson, J., (2005). "Near fault (near field) ground motion effects on reinforced concrete bridge columns." Technical Report No. CCEER-05-07, Center for Civil Engineering Earthquake Research, University of Nevada, Reno, NV.

[6] AASHTO (2002). Standard Specifications for Highway Bridges. American Association of State Highway and Transportation Officials, Washington, D.C.

[7] AASHTO (2014). AASHTO LRFD Bridge Design Specifications. American Association of State Highway and Transportation Officials, Washington, D.C.

[8] Thoen, B. K., & Laplace, P. N. (2004). Offline tuning of shaking tables. In *Proceedings of the 13th World Conference on Earthquake Engineering*.